Research Article

Pavana H* and Rohini Deshpande

"Design and development of magnetic field harvester to power wireless sensors in smart Grid"

https://doi.org/10.1515/ehs-2022-0046
Received May 27, 2022; accepted November 26, 2022;
published online December 12, 2022

Abstract: Real time monitoring of high voltage devices in smart grid is implemented using wireless sensors. They ensure reliable power transfer and avoid cascading power failures. Powering these sensors remotely is a challenge. This paper presents a novel method of powering sensors remotely using magnetic field harvester. A dumbbell shaped magnetic core is designed and optimized to harvest magnetic field near high voltage bus bars/transformers in electrical substation. The harvested power is rectified and boosted. Impedance matching circuit is designed to obtain maximum power transfer to the wireless sensor. The energy thus harvested is used to power wireless sensors and make them self sustainable. The experimental results show that the proposed core with 40,000 turns can harvest 17.6 mW of output power when placed in magnetic flux density of 9 $\mu T_{rms.}$

Keywords: energy harvesting; magnetic core; magnetic field harvester; smart grid; voltage doubler; wireless sensors.

Introduction

In recent times wireless sensors has become an integral part of real time monitoring in smart grid (Chamanian, Baghaee, and Ulusan 2019). Real time monitoring of transmission lines and high voltage devices ensure reliable operation, by monitoring the operating conditions, wear and tear of the devices (Cetinkaya and Akan 2017). Wireless sensors gained prominence due to low power consumption and easy installation in locations that are difficult to access. They are implemented in power grid to measure voltage, current, partial discharge value and temperature. Vibration sensors and line sensors aids in conditional monitoring (Wu, Nguyen, and White 2018).

Wireless sensors are battery operated devices. Lithium ion battery is used as a storage device in sensors. These batteries have typical energy storage capacity of 2800J (Yang et al. 2020). The power consumed by the wireless sensor depends on frequency at which the data is collected and communicated. From the literature survey it is found that low power sensor consumes power around 500 μW to 1 mW (Roscoe and Judd 2013a).

The unpredictable lifetime of the batteries in wireless sensors is the major concern as they are outspread over wide geographical area (Guo, Wang, and Lin 2018). The battery needs replacement regularly which proves to be expensive. In addition to that, lithium ion battery in harsh environment can experience overheating and increase in self discharge (Yang et al. 2020). Often replacement of battery in harsh and widely distributed places is difficult. To overcome this predicament, energy harvesting techniques is implemented to make sensors self-reliant. There are multiple energy sources such as solar, wind, vibration, RF, magnetic field and electric field (Zhu et al. 2009) in power grid that can be harvested. The sources used for harvesting ought to be independent of climatic conditions and should not be time variant (Pavana and Deshpande 2020). As the sensors are used in power grids and are placed near high voltage devices for monitoring, varying magnetic field is the most suitable source of energy. The magnetic field density level in power grid is higher near bus bars, transmission lines, transformer, ripple control systems and switch gears (Roscoe, Judd, and Fraser 2010; Yuan and Huang 2015). Table 1 gives the magnetic flux density near high voltage devices.

Magnetic flux intensity reduces with increase in the distance from the high voltage device (Isokorpi, Keikko, and Korpinen 2002). It is the function of distance from high voltage devices, amount of current flowing through the

***Corresponding author: Pavana H.,** School of Electronics and Communication Engineering, REVA University, Bengaluru, 560064, India, E-mail: pavana62@gmail.com
Rohini Deshpande, School of Electronics and Communication Engineering, REVA University, Bengaluru, 560064, India, E-mail: drrohini.deshpande@gmail.com

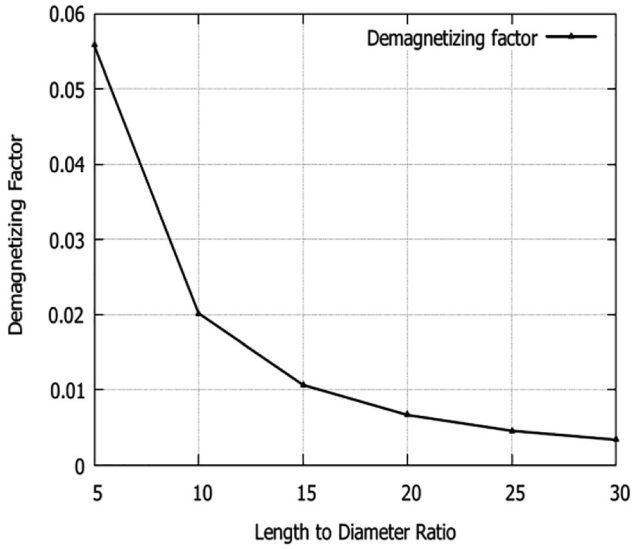

Figure 1: Demagnetizing factor as a function of aspect ratio.

Table 1: Magnetic field near high voltage devices in electric substation.

Sl. No	Test area	Distance from ground	Magnetic flux density
1	110 kV/20 kV switching substations	1 m	18.6 μT (Isokorpi, Keikko, and Korpinen 2002)
2	20 kV cable	0.5 m	14.8 μT (Keikko et al. 2002)
3	110 kV/10 k substation	1.7 m	86.15 μT (Grbic, Pavlovic, and Hrvic 2017)
4	31.5 kV/04 kV transformer	1.5 m	1.7 μT–27 μT (Ozen et al. 2017)
5	400 kV overhead lines	1.25 m	5.16 μT (Oltean et al. 2017)
6	110 kV/35 kV substation	1.5 m	12 μT–20 μT (Grbić, Canova, and Giaccone 2016)

device and distance above the ground. Optimum of these values decides the peak magnetic flux density. According to literature survey summarized in Table 1 maximum flux density of 86.15 μT is found in 110 kV/10 kV substation at 1.7 m above the ground.

Brief review on related work

Magnetic field harvesting system is classified as clamped and non clamped harvester.

(i) Clamped magnetic harvester:

Clamped harvester encloses overhead transmission line carrying huge current. As the core encloses the transmission line, harvested power of the cable clamped harvester is relatively high. The drawback of clamped harvester is that it introduces line sag on the power line. It also provides enormous maintenance risk.

(ii) Non clamped harvester:

These harvesters can be placed anywhere near the high voltage devices in electrical substation (Yuan, Huang, and Zhou 2017). They do not enclose the transmission line and hence are flexible. (Roscoe and Judd 2013a) (Roscoe, Judd, and Fraser 2010) proposed a non clamped magnetic field harvester with cast iron core. The core suffers from eddy current losses, due to the property of cast iron. The core has larger dimensions which increases core volume. (Yuan, Huang, and Zhou 2017) propose ferrite helical shaped core. It is difficult to manufacture helical shaped core in one piece. Multiple pieces are manufactured and glued together to obtain the desired length. This introduces air gap in the core, which reduces harvested power.

The core proposed in this work is simple to construct and can harvest enough energy to power a low power wireless sensor. The core implemented here has no air gap when compared to the previous design. The output from magnetic core is rectified, boosted and regulated in the next stages. Impedance matching circuit is also critical to obtain maximum power transfer (Ferdous and Johnson, 2018a).

Section “Design of magnetic core” deals with design of magnetic core, in Section “Voltage doubler” design of voltage doubler and impedance matching circuits are discussed. Section “Comparison between cylindrical ferrite rod and dumbbell core” deals with comparative analysis between ferrite rod and proposed design. Section “Result and discussion” is dedicated to discussion of results of the proposed magnetic field harvester.

Design of magnetic core

Magnetic core has two parts,

(i) Core

(ii) Winding coil.

Core design

Core material

The proposed core is made of ferrite Mn-Zn. Ferrites are soft magnetic cores. They have high relative permeability, low eddy current and hysteresis losses and high electrical

resistivity (Vieira, Cleonilson, and Molina 2014). The shape of the core is also an important factor in harvester design. Output power is directly proportional to effective permeability and effective permeability depends on shape and dimension of the core. The effective permeability of the gapped core is calculated using Equation (1) (Tashiro, Wakiwaka, and Hattori 2015)

$$\mu_E = \frac{B_{in}}{B_X} \tag{1}$$

Effective permeability increases as length to diameter ratio increases. Effective permeability is related to relative permeability and demagnetizing factor as given in Equation (2) (Tashiro, Wakiwaka, and Hattori 2015). It is inversely proportional to demagnetizing factor.

$$\mu_E = \frac{\mu_r}{1 + N_d \mu_r} \tag{2}$$

where N_d is demagnetizing factor and μ_r is relative permeability of the core. Core with larger length to diameter ratio has less demagnetizing field (Figure 1). But the core becomes brittle when it is long and thin. Hence length to diameter ratio of the core must be optimized. Demagnetizing factor depends on dimension and shape of the core material. Relation between demagnetizing factor and aspect ratio is given by Equation (3).

Demagnetization factor N_d is given by (Tashiro, Wakiwaka, and Hattori 2015)

$$N_d = \frac{1}{\gamma^2 - 1}\left[\frac{1}{\sqrt{\gamma^2 - 1}} \ln\left(\gamma + \sqrt{\gamma^2 - 1}\right) - 1\right] \tag{3}$$

where, γ is the aspect ratio of the core.

The aspect ratio of the core (γ) is the ratio of

It's length to diameter

$$\gamma = \frac{l}{d} \tag{4}$$

where, l is the length of the core and d its diameter.

Figure 1 gives demagnetizing factor as a function of aspect ratio.

It can be seen from the above graph that demagnetization factor reduces with increase in the length to diameter ratio. However when the length to diameter ratio is increased; the core becomes long and thin. This reduces the ruggedness of the core. Therefore it must be optimized.

Losses in magnetic core

Losses in the magnetic core are due to resistance offered by magnetic core and the copper coil. The total resistance offered by the magnetic core is given below

$$R = R_{Core} + R_{Coil} \tag{5}$$

Core losses: These losses are due to the nature of alternating magnetic field surrounding the magnetic core. Core loss consists of eddy current and hysteresis losses (Vishay Intertechnolog INC). Hysteresis losses are the function of frequency and magnetic field (Yuan, Huang, and Zhou 2017). The frequency of the magnetic field is very low (50 Hz), in addition the magnetic fields around high voltage devices are in the order of milli Tesla. Hence hysteresis losses are ignored.

Eddy current loss depends on electrical resistivity of the core material and diameter of the core material. Power loss due to eddy current is given in Equation (6) (Espe and Mathisen 2020)

$$P_{eddy} = \frac{\pi^2 f^2 d^2 B^2}{16\rho} \tag{6}$$

where d is the diameter of the rod, f is the frequency; B is magnetic flux density, ρ is the resistivity of the core material.

Ferrite Mn-Zn core has high electrical resistivity in the order of 1.1 MΩm (Byte 2011) and in addition the core diameter in the proposed work is small. From Equation (5) it is seen that eddy current losses are directly proportional to diameter and inversely proportional to electrical resistivity of the core. Hence the eddy current losses are negligible and are ignored. Therefore the total loss in the proposed harvester is due to resistance offered by the copper coil wounded on the magnetic core.

Equivalent circuit of the magnetic core is given in Figure 2.

L_{coil} is inductance of the coil and R_{coil} is resistance offered by the coil. v_{ac} is the induced voltage.

According to Faraday's law of electromagnetic induction, when the magnetic core is placed in the varying magnetic field, alternating voltage is induced in the coil. The voltage thus induced is given in Equation (7) (Roscoe and Judd 2013a).

$$V_{ac} = 2(\pi r)^2 f B N \mu_E \tag{7}$$

where f is Frequency of the magnetic field,

μ_E is effective permeability, r is radius of the core. B is Magnetic Flux density, N is Number of turns.

The output power across the load is calculated as below

$$P_{out} = \frac{(V_{ac})^2}{4R} \tag{8}$$

Output power per unit volume can be calculated using Equation (10). And the volume of the magnetic core is given below

$$\text{Volume} = \pi r^2 l \tag{9}$$

$$P_{\text{out}} = \frac{(2\pi^2 f r^2 B N \mu_{\text{E}})^2}{4\text{R}\pi r^2 l} \tag{10}$$

The maximum power is transferred to load when the input impedance matches the output impedance. Hence impedance matching circuit plays an important role.

Coil design

Copper coil wounded on the magnetic core plays an important factor in harvesting.

$$V_{\text{ac}} = 2(\pi r)^2 f B N \mu_{\text{E}} \tag{11}$$

From the equation above, output voltage is directly proportional to number of turns. However, increase in number of turn N, increases coil resistance. Resistance of the copper coil is calculated using the below equation

$$R_{\text{total}} = \frac{\rho l}{A} \tag{12}$$

where ρ is the resistivity of the core, L is the length of the core and A is the area of the core.

The total wire length is given by (kiziroglou, Wright, and Yeatman 2020)

$$L_{\text{wire}} = 2\pi N\left(D + \left(J_{\text{layer}} \times d\right)\right) \tag{13}$$

where D is the diameter of the core, N is number of turns, J_{layer} is number of layers wounded and d is the diameter of the wire. J_{layer} is number of layers wounded, W is width of copper coil. (kiziroglou, Wright, and Yeatman 2020).

$$J_{\text{layer}} = \frac{\text{N}}{(\text{W}/\text{d})} \tag{14}$$

Resistance of the copper coil is directly proportional to the length of the coil. And length of the coil depends on number of turns. Hence increase in number of turns, increases the resistance. From the Figure 3 it is seen that core with larger inner diameter offers more resistance as the number of turns increases. Hence the diameter of the core must be optimized. D_{in} is varied by keeping length of the core L constant. Rod(a) = 2 cm, Rod(b) = 2.5 cm,

Rod(c) = 3 cm, Rod(d) = 3.5 cm, Rod(e) = 4 cm, Rod(f) = 4.5 cm and Length L = 25 cm.

The diameter of the copper wire used is an important factor. Figure 4 gives the relationship between diameter of the coil as the function of resistance for different number of turns. It can be seen from the below graph that, the wire with larger diameter has less resistance.

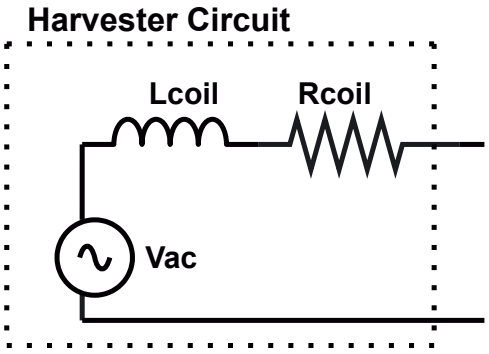

Figure 2: Magnetic core equivalent circuit.

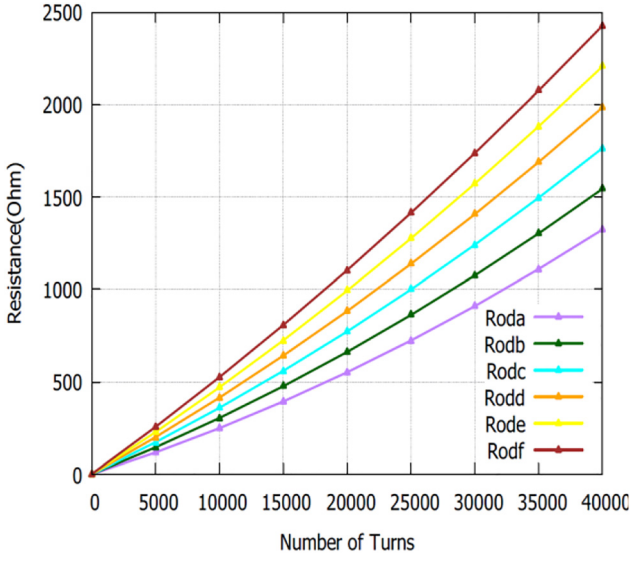

Figure 3: Coil resistance as a function of number of turns.

From the above graph it can be seen that larger number of turns offers more resistance. In addition for the given number of turns, as the diameter of copper coil increases,

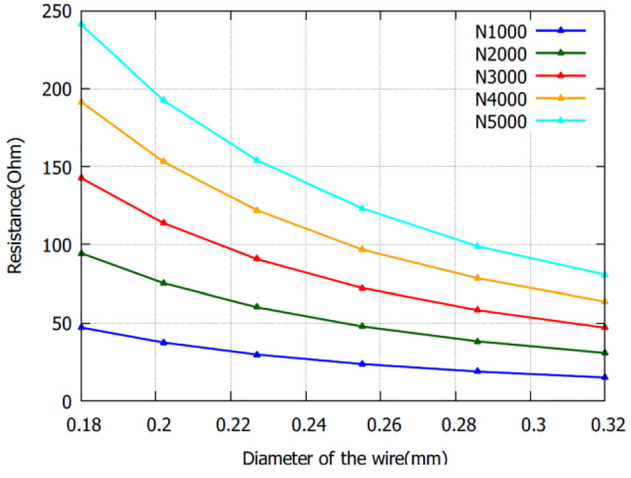

Figure 4: Coil resistance as the function of wire diameter.

resistance decreases. However copper coil with larger diameter occupy more area in the core and hence reduces the number of turns. Figure 5 gives number of turns as the function of wire diameter.

From the Figure 5 it is seen that when wire with larger diameter is wounded on the core, it occupies more area and number of turns tends to decrease. The voltage induced on the coil is proportional to number of turns. Copper wire with smaller diameter increase the number of turns as the space occupied by them is less. However they offer large resistance. Hence an optimum wire diameter must be chosen. The wire chosen in the proposed work has the diameter of 0.255 mm and resistivity of 0.352 Ω/m.

Simulation of cylindrical rod

Cylindrical ferrite rod with length L and diameter Din and relative permeability of 2300 is placed in the uniform magnetic field of 9 μT_{rms} (Figure 6). Magnetic field of 9 μT_{rms} is generated using Helmholtz coil in CST EM Studio.

Magnetic flux density in the middle of the cylindrical ferrite rod is measured for different length to diameter ratio. The Table 2 gives the simulated and measured output for different aspect ratio of the ferrite rod.

From the above simulated result it is seen that, with the increase in the diameter of the rod output power increases. In addition the resistance offered by the coil increases.

The ferrite core is simulated and magnetic field density is measured in the middle of the core (Figure 6). Effective permeability is calculated using Equation (1). Figure 7 gives the relationship between effective permeability and relative permeability for different length to diameter ratio of the ferrite rod. Length of the core is kept constant L = 25 cm. D_{in} of the core is varied. Rod(a) = 2 cm, Rod(b) = 2.5 cm, Rod(c) = 3 cm, Rod(d) = 3.5 cm, Rod(e) = 4 cm, Rod(f) = 4.5 cm.

Table 2: Parameters of the cores for different diameter and when μ_r = 2300, N = 200, L = 25 cm. D_{in} of the core is varied. Rod(a) = 2 cm, Rod(b) = 2.5 cm, Rod(c) = 3 cm, Rod(d) = 3.5 cm, Rod(e) = 4 cm, Rod(f) = 4.5 cm.

Core	μ_E	N_d	V_{Coil} (mV)	V_O (mV)	R_{Coil} (Ω)	P_{out} (μW)
Rod(a)	87.1	0.011	15	7.5	4.4	13.5
Rod(b)	63.3	0.016	17.5	8.7	5.5	13.9
Rod(c)	48.7	0.020	19.4	9.7	6.6	14.3
Rod(d)	39.3	0.026	21.3	10.6	7.7	14.7
Rod(e)	32.8	0.031	23.3	11.6	8.8	15.4
Rod(f)	28.1	0.036	25.2	12.6	9.9	16

From the graph above it is seen that effective permeability increases with increase in relative permeability of the core material. And after certain value, effective permeability becomes independent of relative permeability and will not provide any significant raise.

The core used here is Mn-Zn which has relative permeability of 2300. From the above simulated result it is found that maximum power is harvested when ferrite rod is long and thin. Long and thin core increases the distance between North Pole and South Pole of the magnetic core hence demagnetization decreases (Yuan, Huang, and Zhou

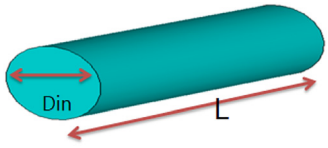

Figure 6: Cylindrical ferrite rod.

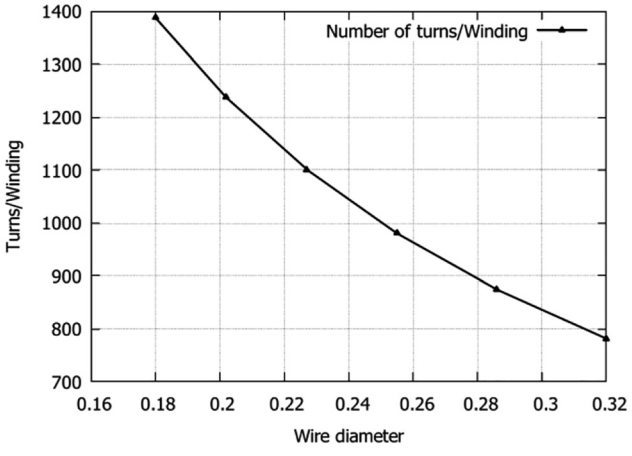

Figure 5: Number of turns as the function of wire diameter.

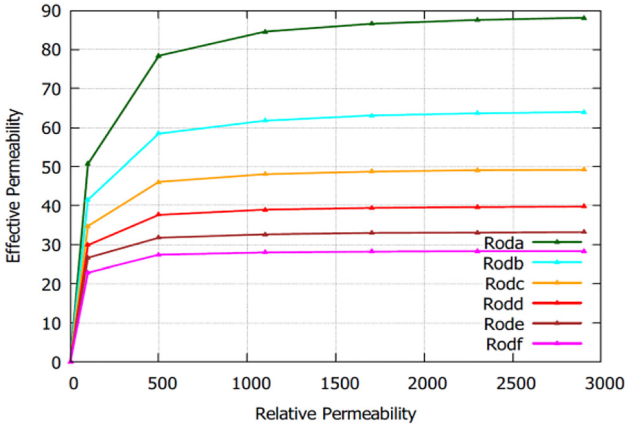

Figure 7: Effective permeability as a function of relative permeability for different length to diameter ratio.

2017). Long and thin ferrite core is brittle and is prone to be damaged. It is seen from Table 2 that the there is a slight increase in output power with increase in the diameter of the core. With the increase in the core diameter, coil resistance increases for larger number of turns. Hence length to diameter of the core must be optimized.

Design of dumbbell magnetic core

From the above discussion it is seen that increase in length to diameter ratio increases power harvested from the core. Long and thin core tends to be very brittle and there is a chance of breaking. Hence to increase the flux linkage to the ferrite rod, magnetic plates are added. Figure 8 is the proposed magnetic core.

D_{in} is the inner diameter of the core, L is the length of the core, D_{out} is the outer diameter of the magnetic plate, and W is the width of the magnetic plate.

Simulation of dumbbell core

Dumbbell shaped core with $D_{in} = 2$ cm, $L = 25$ cm, $W = 2.6$ cm is simulated in CST EM studio with the flux density of 9 μT_{Rms} The number of turns $N = 200$ and relative permeability is 2300. The diameter of outer plate is varied keeping width of the magnetic plate constant. The simulated result is tabulated in Table 3.

It is observed from the above simulation results that, as the diameter of magnetic plate increases for the given aspect ratio of the core, the output power increases. However the resistance remains constant. Figure 9 gives core diameter as function of output power when the diameter of the magnetic plate is varied

It is seen from the simulated result that maximum power is harvested when dumbbell core has greater aspect ratio and magnetic plate with larger diameter. Table 4 gives simulated results of dumbbell shaped rod with $D_{in} = 2$ cm, $L = 25$ cm. The number of turns $N = 200$ and Relative permeability is 2300. The $D_{out} = 11$ cm and the width of the outer plate W is varied.

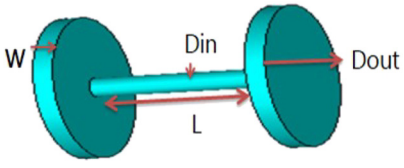

Figure 8: Dumbbell core.

Table 3: Parameters of the cores for different diameter and when $\mu_r = 2300$, N = 200. D_{out} is varied. Rod(a) = 10 cm, Rod(b) = 12 cm, Rod(c) = 14 cm, Rod(d) = 16 cm, Rod(e) = 18 cm, Rod(f) = 20 cm.

Core	μ_E	N_d	V_{Coil} (mV)	V_O (mV)	R_{Coil} (Ω)	P_{out} (μW)
Rod(a)	251.1	0.0039	44.6	22.3	4.4	112.5
Rod(b)	290.6	0.0034	51.6	25.8	4.4	150.8
Rod(c)	328.8	0.003	58.4	29.2	4.4	193.0
Rod(d)	367.7	0.0027	65.3	32.6	4.4	241.4
Rod(e)	407.7	0.0024	72.4	36.2	4.4	296.8
Rod(f)	477.7	0.0022	84.8	42.3	4.4	407.4

It can be seen from the above simulated results that output power increases with the increase in the width of the magnetic plate. The output power density depends on the induced voltage, coil resistance and core volume (Roscoe

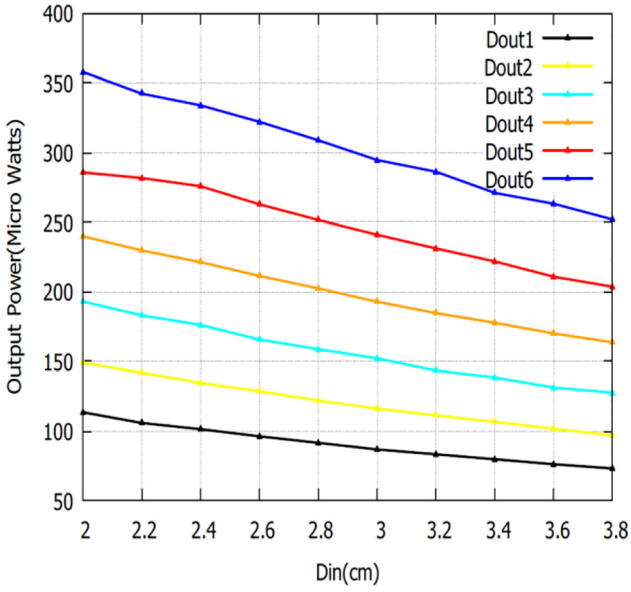

Figure 9: The output power of dumbbell core as the function of diameter D_{in}.

Table 4: Parameters of the cores for different diameter and when $\mu_r = 2300$, $N = 200$. W is varied. Rod(a) = 2 cm, Rod(b) = 2.5 cm, Rod(c) = 3 cm, Rod(d) = 3.5 cm, Rod(e) = 4 cm, Rod(f) = 4.5 cm.

Core	μ_E	N_d	V_{Coil} (mV)	V_O (mV)	R_{Coil} (Ω)	P_{out} (μW)
Rod(a)	253.3	0.003	45	22.5	4.4	114.5
Rod(b)	265.5	0.0037	47.1	23.5	4.4	125.7
Rod(c)	278.8	0.0036	49.5	24.7	4.4	138.8
Rod(d)	298.8	0.0035	53	26.5	4.4	159.4
Rod(e)	303.3	0.0033	53.8	26.9	4.4	164.1
Rod(f)	316.6	0.0031	56.2	28.1	4.4	178.9

and Judd 2013a). Optimal value of length to diameter ratio and dimensions of magnetic plate should be selected to maximize the output power density. The output voltage from the magnetic core is alternating in nature. It must to be rectified, amplified and regulated before sending it to the load.

Voltage doubler

Voltage doubler is a device used to rectify AC to DC and also to boost the output voltage (Mohammed and Sari 2019). It is essential to implement voltage doubler in harvester as the output from magnetic core is low. Single stage Greinacher voltage doubler is designed to boost output voltage. Greinacher voltage doubler generates high DC voltage from the low AC voltage signal (Rani, Kaur, and Bhatia 2017). It has two diodes and two capacitors. The diode used must have lowest switching time and low threshold voltage. Schottky diode is used due its low voltage drop, low conduction loss and small reverse current (Sathyiyapriya et al. 2020). The Schottky diode PMEG2020AEA with forward voltage drop of 0.19 V is used here. Impedance matching circuit is critical in obtaining the maximum power transfer in the harvester (Ferdous and Johnson, 2018b). *L* shaped impedance matching circuit is designed to obtain maximum efficiency (Fan, Gou, and Zhao 2019). Voltage doubler with impedance matching circuit is designed in Figure 10.

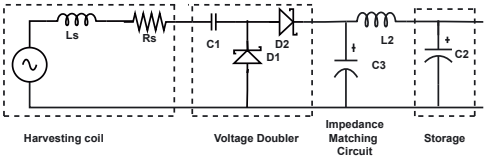

Figure 10: Voltage doubler.

The capacitor C1 present has two functions. It compensates self inductance of the coil. And in addition it acts as one of the capacitor in voltage doubler. The capacitor C2 acts as smoothing capacitor and storage device. The inductance of the harvesting core can be compensated by a series capacitance at frequency of 50 Hz using the equation below (Roscoe and Judd 2013b).

$$C_1 = \frac{1}{\omega^2 L_S} \tag{15}$$

The circuit is simulated using LT Spice for different values of capacitor C1 for parameters in Table 5. The graph is plotted for output power as the function of compensating capacitance C1.

Table 5: Parameters of magnetic core.

Parameters	Value
Coil voltage	9.98 Vrms
Number of turns	40000
Coil resistance	1400
Coil inductance	683

Output power as a function of capacitance C1 is plotted (Figure 11). It can be seen from the below graph that maximum output is obtained when the inductance of the magnetic core compensated using capacitor. The value of the capacitance is calculated from Equation (14).

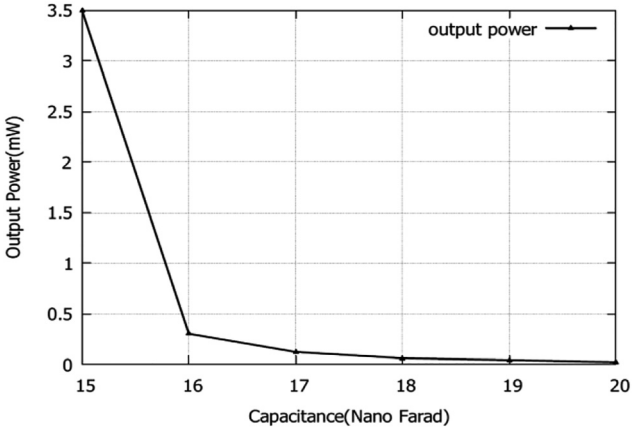

Figure 11: Output power as the function of compensating capacitor.

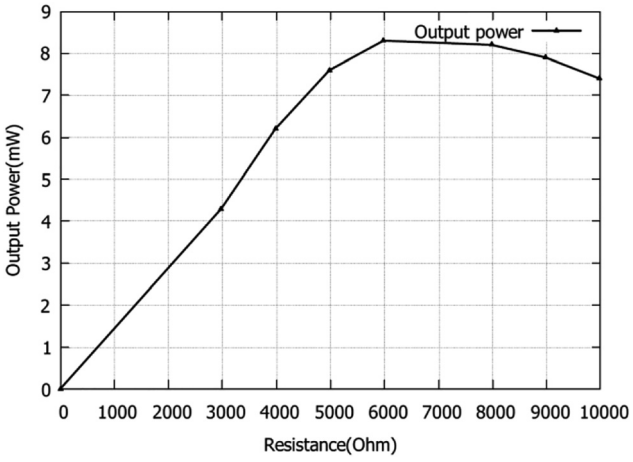

Figure 12: The output power as the function of resistance.

Using LT Spice output power for different load values is simulated. It is found that maximum power is transferred when the load is approximately 4 times larger than the source resistance. Figure 12 gives the relationship between output power as the function of load resistance. Maximum output power is obtained at 5.9 KΩ which is approximately 4 times greater than the coil resistance 1400 KΩ considered.

Comparison between cylindrical ferrite rod and dumbbell core

Uniform Magnetic field can be generated using Helmholtz coil where ferrite core is placed. The boundary condition is set to open. Helmholtz coil is shown in Figure 13 (Saqib, Francis, and Francis 2020).

Helmholtz coil has two identical magnetic coil coils with radius R. They are separated from the distance R. It is equal to the radius of the coil.

The flux density generated by the Helmholtz coil is calculated as below (Saqib, Francis, and Francis 2020)

$$B = \frac{\mu_0 8NI}{R\sqrt{125}} \tag{16}$$

where μ_0 is permeability of free space

N is the number of turns wounded.

I is current through the coil, in amperes.

R is the radius of the Helmholtz coil, in meters.

The copper coil used to build Helmholtz is 0.5 m and the number of turns used here is 40. The current through each coil is 125 mA. The flux density generated is 9 μT. The Helmholtz coil is simulated in CST EM Studio. The ferrite core is place in the magnetic field density of 9 μT.

Cylindrical ferrite rod with relative permeability of 2300 is simulated in CST EM Studio. Inner diameter (D_{in}) of rod is varied and output power is plotted for different number of turns. The copper coil wounded on the magnetic core has a diameter 0.255 mm and resistivity of 0.352 Ω/m. D_{in} is varied. L = 25 cm, μ_r = 2300

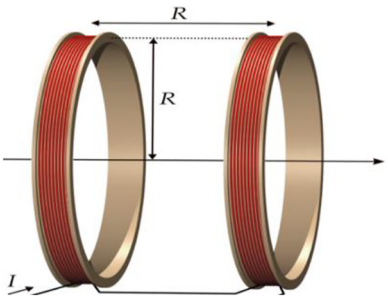

Figure 13: Helmholtz coil.

Rod(a) = 2 cm, Rod(b) = 3 cm, {Rod(c) = 4c}.

It can be seen from Figure 14, with the increase in the diameter of the ferrite rod there is a small increase in output power. Along with output power the resistance offered by the core increases. The output power of the ferrite rod with diameter 2 cm and N = 2000 is 13.5 μW. To further increase the flux linkage to the core, magnetic plate is added to the ferrite rod. Dumbbell core is designed and simulated for different dimensions. It is simulated and output power as the function of number of turns is plotted by varying inner diameter (D_{in}). Rod(a) = 2 cm, Rod(b) = 3 cm, Rod(c) = 4 cm. D_{out} = 11 cm, W = 2.8 cm is kept constant.

It is seen from Figure 15 that the dumbbell core with small inner diameter generate more output. The output power for dumbbell core with core diameter of 2 cm, length L = 25 cm, width of the magnetic plate W = 2.6 cm and

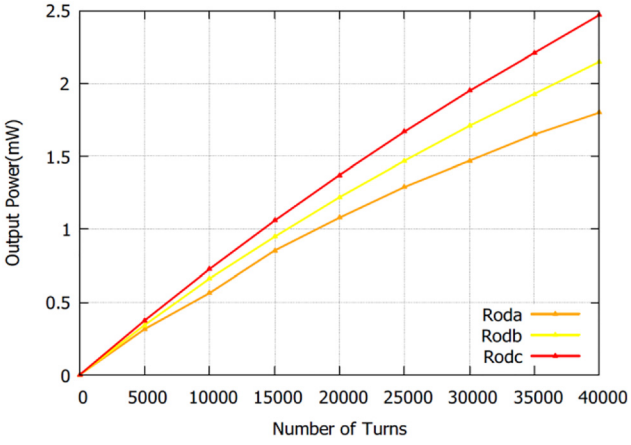

Figure 14: Output power as function of number of turns in cylindrical rod.

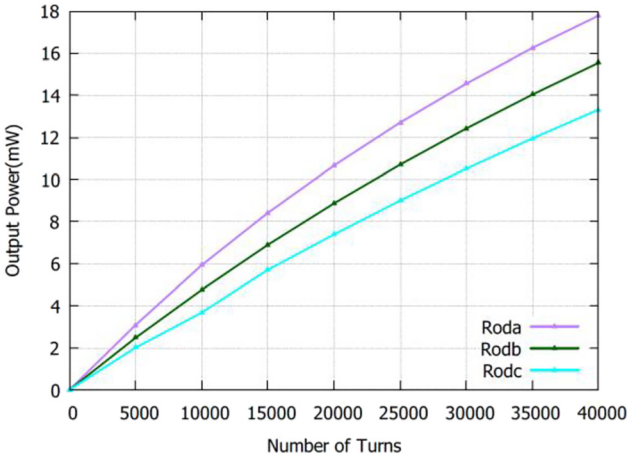

Figure 15: Output power as function of number of turns in dumbbell core.

D_{out} = 12 cm for N = 2000 is 112.56 μW. It is seen from the Figures 14 and 15 that the output from dumbbell core is much larger than the cylindrical rod for the given diameter. The magnetic plate attached to the ferrite core increases the flux linkage and hence flux density inside the core is increased which in turn increases the output power.

Result and discussion

The proposed dumbbell core is designed and simulated using CST EM Studio. Dumbbell Core with Inner diameter D_{in} = 2.2 cm, L = 25 cm and D_{out} = 11 cm and width W = 2.8 cm is designed and simulated in the flux density of 9 μT. Wire diameter 0.255 mm and resistivity of 0.352 Ω/m is considered. The output power for different number of turns is simulated and plotted (Table 6 and Figure 16).

The output power harvested for the proposed core is 1.25 mW and power density is 1.99 μW/cm3 for 2000 number of turns. For 40,000 turns the output power harvested is 17.63 mW. As the number of turns is increased the output power increases (Figure 16). If the harvester is placed near higher flux density, more power can be harvested.

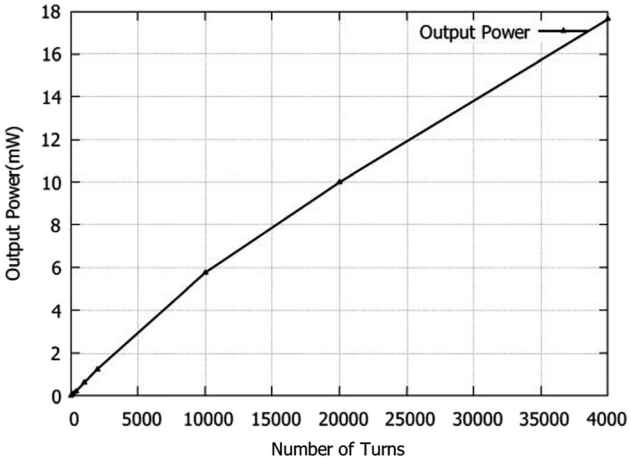

Figure 16: The output power as function of different number of turns is plotted.

Table 6: Simulated results for different number of turns.

Number of turns	Open circuit voltage	Output power
200	49 mV	0.12 mW
2000	499 mV	1.25 mW
20000	4.99 V	10 mW
40000	9.98 V	17.63 mW

The Output voltage from harvester is alternating in nature; hence it is rectified and increased using voltage doubler to meet the voltage requirement of wireless sensor. Impedance matching circuit is designed to obtain the maximum power transfer. The proposed impedance matching circuit provides energy conversion efficiency of 77% which is higher than the previous design.

Conclusions

In this paper dumbbell shaped core is designed to harvest magnetic field near high voltage devices in electrical substation. The output from the core is rectified and doubled using voltage doubler. Impedance matching circuit is designed to maximize the power transfer efficiency from core to load. The energy conversion efficiency is here 77%. The proposed core is not clamped on to the power line and hence can be placed near high voltage devices. It has magnetic plate connected to the cylindrical rod that increases the flux linkage and hence increases the harvested power. The core designed here is simple in construction when compared to the previous design. From the results it is shown that the output power density of the dumbbell core with 40,000 turns is 17.6 mW enough to power any low power sensors.

Author contributions: All the authors have accepted responsibility for the entire content of this submitted manuscript and approved submission.
Research funding: Authors acknowledge the support from REVA University for the facilities provided to carry out the research. Authors also thank the reviewers for their useful constructive comments.
Conflict of interest statement: The authors declare no conflicts of interest regarding this article.

References

Byte Mark. 2011. *Nanocrystalline cores* [online]. http://www.bytemark.com/products/Nanocrystalline_cores.html (accessed August 20, 2021).

Cetinkaya, O., and O. B. Akan. 2017. "Electric-Field Energy Harvesting in Wireless Networks." *IEEE Wireless Communications* 24 (2): 34–41.

Chamanian, S., S. Baghaee, and H. Ulusan. 2019. "Implementation of Energy-Neutral Operation on Vibration Energy Harvesting WSN." *IEEE Sensors Journal* 19 (8): 3092–9.

Espe, A. E., and G. Mathisen. 2020. "Towards Magnetic Field Energy Harvesting Near Electrified Railway Tracks." In *2020 9th Mediterranean Conference on Embedded Computing*, 8–11.

Fan, S., W. Gou, and Y. Zhao. 2019. "A 2.45-GHz Rectifier-Booster Regulator with Impedance Matching Converters for Wireless Energy Harvesting." *IEEE Transactions on Microwave Theory and Techniques* 67 (9): 3833–43.

Ferdous, M. S., and T. Johnson. 2018a. "A Power Scavenging Current Transformer to Remotely Power 'bird on Wire' Sensors in Grid Monitoring." In *IEEE Wireless Power Transfer Conference (WPTC)*, 3–7.

Ferdous, M. S., and T. Johnson. 2018b. "A Power Scavenging Current Transformer to Remotely Power 'bird on Wire' Sensors in Grid Monitoring." In *IEEE Wireless Power Transfer Conference (WPTC)*, 3–7.

Grbić, M., A. Canova, and L. Giaccone. 2016. "Levels of Magnetic Field in an Apartment Near 110/35 KV Substation and Proposal of Mitigation Techniques." In *Mediterranean Conference On Power Generation, Transmission, Distribution and Energy Conversion (MedPower 2016)*, 6–9.

Grbic, M., A. Pavlovic, and D. Hrvic. 2017. "Levels of Electric and Magnetic Fields inside 110/x kV Substation." *IET Journal* 2017 (1): 747–51.

Guo, S., P. Wang, and J. Lin. 2018. "Power Harvesting Technologies in the Power Grid." In *2018 China International Conference on Electricity Distribution*, 17–9.

Isokorpi, J., T. Keikko, and L. Korpinen. 2002. "Power Frequency Electric and Magnetic Fields at a 110/20 kV Substation." In *PowerTech Budapest IEEE Conference*.

Keikko, T., S. Kuusiluoma, T. Sauramaki, and L. Korpinen. 2002. "Comparison of Electric and Magnetic Fields Near 400 kV Electric Substation with Exposure Recommendations of the European Union." In *IEEE/PES Transmission and Distribution Conference and Exhibition*, 6–10.

kiziroglou, M. E., S. W. Wright, and E. M. Yeatman. 2020. "Coil and Core Design for Inductive Energy Receivers." *Sensors and Actuators A: Physical Elsevier* 313 (2020): 112206.

Mohammed, M., and F. Sari. 2019. "Analysis of Dickson Voltage Multiplier for RF Energy Harvesting." In *IEEE Global Power, Energy and Communication Conference*.

Oltean, M. N., T. Fagarasan, G. Florea, C. Munteanu, and A. Pop. 2017. "Electromagnetic Field Measurement on High Voltage Overhead Lines." In *2017 12th International Conference On Live Maintenance (ICOLIM)*, 26–8.

Ozen, S., H. F. Carlak, O. H. Colak, and S. Helhel. 2017. "Magnetic Field Risk Analysis for Employees and Patients Due to Power Transformers in Hospital Buildings." In *2017 Progress in Electromagnetics Research Symposium – Spring (PIERS) IEEE*, 22–5.

Pavana, H., and Dr. R. Deshpande. 2020. "Energy Harvesting Techniques for Monitoring Devices in Smart Grid Application." In *2020 Third International Conference On Advances in Electronics, Computers and Communications (ICAECC)*, 11–2.

Rani, N., J. Kaur, and H. Bhatia. 2017. "Design and Performance Analysis of Cockroft-Walton Voltage Multiplier (CWVW) Energy Harvesting for Low Power Application." In *Electromagnetics Research Symposium-Spring*.

Roscoe, N. M., and M. D. Judd. 2013a. "Harvesting Energy from Magnetic Fields to Power Condition Monitoring Sensors." *IEEE Sensors Journal* 13, https://doi.org/10.1109/jsen.2013.2251625.

Roscoe, N. M., and M. D. Judd. 2013b. "Optimization of Voltage Doublers for Energy Harvesting Applications." *IEEE Sensors Journal* 13, https://doi.org/10.1109/jsen.2013.2278468.

Roscoe, N. M., M. D. Judd, and I. Fraser. 2010. "A Novel Inductive Electromagnetic Energy Harvester for Condition Monitoring Sensors." In *CMD2010*, 615–8. Tokyo: IEEE Electrical Insulation Magazine.

Saqib, M., S. N. Francis, and J. N. Francis. 2020. "Design and Development of Helmholtz Coils for Magnetic Field." In *2020 International Youth Conference on Radio Electronics, Electrical and Power Engineering (REEPE)*, 1–5.

Sathyiyapriya, T., V. Gurunathan, K. N. Krishna Prasad, and T. N. Kumar. 2020. "VoltageDoubler Design for RF Energy Harvesting System." In *IEEE 7th International Conference on Smart Structures and Systems ICSSS*.

Tashiro, K., H. Wakiwaka, and G.Y. Hattori. 2015. "Estimation of Effective Permeability of Dumbbell-Shaped Magneticcore." *IEEE Transactions on Magnetics* 51 (1): 1–4.

Vieira, D. A., Cleonilson, and Y. P. Molina. 2014. "Energy Harvesting Using Magnetic Induction Considering Different Core Materials." In *IEEE Instrumentation and Measurement Technology Conference*.

Vishay Intertechnology INC. Inductors Instructional Guide. [online]. Also available at https://www.vishay.com/docs/49782/49782.pdf.

Wu, Z., D. S. Nguyen, and R. M. White. 2018. "Electromagnetic Energy Harvester for Atmospheric Sensor on Overhead Power Distribution Lines." *IOP Conference Series: Journal of Physics* 1052 (2018): 012081.

Yang F, Du L, Yu H, Huang P. 2020. Magnetic and Electric Energy Harvesting Technologies in Power Grids: A Review. Sensors (Basel) 20 (5): 1496. PMID: 32182831

Yuan, S., and Y. Huang. 2015. "Magnetic Field Energy Harvesting under Overhead Power Lines." *IEEE Transactions on Power Electronics* 30 (11): 6191–202.

Yuan, S., Y. Huang, and J. Zhou. 2017. "A High-Efficiency Helical Core for Magnetic Field Energy Harvesting." *IEEE Transactions on Power Electronics* 32 (7): 5365–76.

Zhu, M., M. D. Judd, P. J. Moore, and R. Zhang. 2009. "Energy Harvesting Techniques for Powering Autonomous Sensors within Substations." In *2009 International Conference On Sustainable Power Generation and Supply*, 6–7.